Deuteron-production double-differential cross sections for 300- and 392-MeV proton-induced reactions deduced from experiment and model calculation

Yusuke Uozumi,* Yusuke Sawada, Aleksandre Mzhavia, and Sho Nogamine
Department of Applied Quantum Physics and Nuclear Engineering, Kyushu University, 744 Motooka, Nishi-ku, Fukuoka 819-0395, Japan

Hiroki Iwamoto and Tadahiro Kin
Japan Atomic Energy Agency, Tokai-mura, Naka-gun, Ibaraki 319-1195, Japan

Shinya Hohara and Genichiro Wakabayashi
Kinki University Atomic Energy Research Institute, Kowakae, Higashiosaka 577-8502, Japan

Masahiro Nakano
Junshin Gakuen University, 1-1-1 Chikushigaoka, Minami-ku, Fukuoka 815-8510, Japan
(Received 24 May 2011; published 27 December 2011)

Deuteron production from intermediate-energy proton-nucleus interactions was investigated through experiments and model calculations, mainly to develop a theoretical model by elucidating the mechanism of cluster production. Spectral double-differential cross sections were measured for inclusive (p, dx) reactions on five targets in the periodic table, namely ^{12}C, ^{27}Al, ^{51}V, ^{93}Nb, and ^{197}Au, at beam energies of 300 and 392 MeV. The cross sections were determined in almost the entire outgoing energy range from the highest down to 30 MeV and at laboratory angles from 20° to 104°. To interpret the measured spectra, we proposed a new model that includes the nucleon correlations of the initial- and final-state interactions to describe cluster knockout and pickup within the intranuclear cascade model. The results of the model calculations showed reasonable agreements with those of the experiments. Moreover, the model indicated reasonable predictive power for the $(p, ^3\mathrm{He}x)$, $(p, \alpha x)$, and $(d, d'x)$ reactions measured elsewhere. The quantum molecular dynamics model underpredicts the results of the experiments by two to three orders except for low-energy portions of the (p, dx) spectra.

DOI: 10.1103/PhysRevC.84.064617 PACS number(s): 25.40.Ep, 25.40.Sc, 29.40.Mc

I. INTRODUCTION

The production of particles from intermediate-energy proton-nucleus interactions has been extensively studied for many years. As for nucleon production, its mechanism is understood rather well and prediction of energy-angle double-differential cross sections (DDXs) is possible with satisfactory accuracy. Nucleon emission from the cascade phase is well described by the intranuclear cascade (INC) and quantum molecular dynamics (QMD) models. For nucleon emission from the second slow phase, the evaporation model has been established. These models are now incorporated in macroscopic transport simulation tools, such as PHITS [1] and GEANT4 [2], and play an essential role in developing various technologies, for instance, accelerator-driven systems and particulate radiation therapy.

The production of light clusters, such as d and α, has been intensively investigated. The slow phase can be well described by the evaporation model with statistical computation. However, high-energy cluster emission processes remain to be elucidated, and no theoretical model is as yet available for predicting DDXs. Extensive effort is necessary toward understanding the mechanisms of cluster production by experiments and theoretical model calculations.

Although the mechanism of cluster production from nucleon-induced reactions has been investigated intensively, crucial questions remain [3]. The reaction giving rise to α-cluster emission has attracted particular attention and many theoretical models have been proposed to unravel the mechanism involved in such a reaction. A large number of them are based on exciton or hybrid models and have focused on two different mechanisms. The first involves an indirect knockout of a preformed cluster, and the second involves coalescence or pickup, in which a cluster is formed in the course of reaction. We consider that beam energies below 100 MeV may be too low to distinguish the roles of knockout and pickup processes; however, in the higher-energy domain, the roles of these processes can be distinguished by calculations. Moreover, the exciton model does not take angular momentum into account and, therefore, does not consider angular distributions, which are among the most important physical quantities. It is clear that the classical cluster-knockout picture has difficulty in accounting for the forward peak in experimental angular distributions; nevertheless, this is intuitively expected to influence higher-energy cluster production.

The QMD and antisymmetrized molecular dynamics (AMD) models are also candidates for describing cluster production. Cluster production lies within the framework of molecular dynamics and, thus, may be considered to be a natural application of such models. AMD has been studied and is reported to reasonably describe [4] the α-cluster energy

*uozumi@nucl.kyushu-u.ac.jp

TABLE I. Targets used in this work.

	C	Al	V	Nb	Au
Thickness (mg/cm^2)	33	27	2.5	43	19

distribution resulting from collisions between heavy ions with energies of approximately 30 MeV/u. However, such a study was carried out in the case where the nucleon momentum was small relative to the center of mass of the system, and in such a scenario cluster formation should be governed by a coalescence-like process. In fact, the coalescence model [5–7] can reproduce the lower-energy part of the spectrum, but not the higher-energy part. Nevertheless, there have been no successful attempts to model the high-energy portions of the spectra, due to heavy-ion collisions and proton-induced reactions. The mechanism involved in high-energy deuteron production has remained an open question because of the very small binding energy involved. In these cases, the clustering process must overcome a large momentum difference by quantum mechanisms, and QMD and AMD lose their predictive power.

The INC model describes reactions in terms of only two-body collisions and does not consider cluster production. To describe cluster production, the INC model must incorporate phenomenological treatment of nucleon correlations. Thus far, this approach has been followed in a few studies. Percolation [8] was introduced at the end of the cascade phase, and, more recently, surface coalescence [9,10] was incorporated during this phase. However, the studies concluded [11,12] that surface coalescence needs further improvement for predicting absolute DDXs. Since the coalescence approach is insufficient to explain the high-energy range, we consider that a new approach, including the knockout process, is indispensable to interpret the entire range of spectra. Although the exciton model treats a preformed cluster as an elemental particle, to include such a boson in the INC model is nontrivial. In a new model of knockout, a preformed cluster should be treated as a strongly correlated nucleon pair, not as an elemental particle.

In this work, we investigate deuteron production. To this end, a systematic set of experimental data is essential. Previously obtained data are mainly below 100 MeV, which is too low to distinguish knockout and pickup contributions.

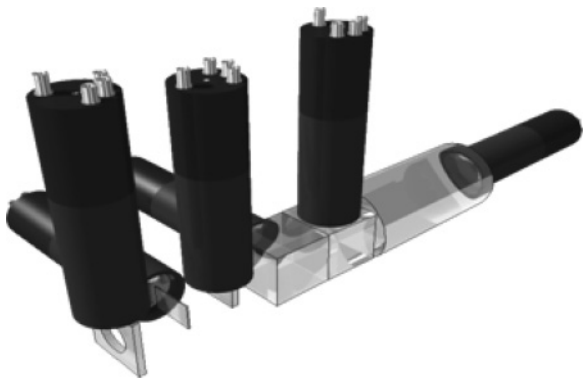

FIG. 1. Schematic of the detector.

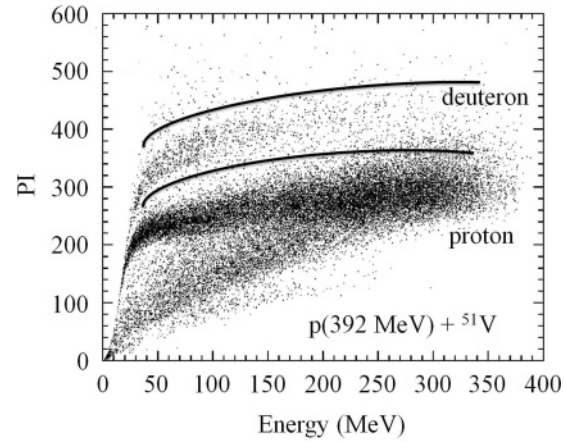

FIG. 2. Two-dimensional PI plot for the $p + {}^{51}$V reaction at 30° and incident energy equal to 392 MeV.

Although there are several data sets in the energy domain above 300 MeV [11–16], they are insufficient for discussing the general trend of the reaction in detail because of the narrow ranges of energies and angles of measured deuterons. The data of 300–400 MeV have an advantage: The real part of the nuclear optical potential is very weak, and the NN cross sections reach their minimum; hence, the incident proton travels in an almost straight line and reaches deep inside the target nucleus. Furthermore, the reaction process can be described within the nucleon degrees of freedom, since pion production remains negligible. These experimental data offer a good opportunity for examining the predictive capability of the new model.

In this study, DDXs of inclusive (p, dx) reactions are investigated to decipher the broad features of proton-induced reactions. The INC model is extended to describe deuteron production, and its validity is examined. Five targets, namely ^{12}C, ^{27}Al, ^{51}V, ^{93}Nb, and ^{197}Au, are chosen to cover a wide range of masses in the periodic table. The proton beam energies chosen are 300 and 392 MeV, which are expected to clarify the roles of knockout and pickup processes. The model study is pursued for other cluster emission reactions, such as $(p, {}^3\mathrm{He}x)$, $(p, \alpha x)$, and $(d, d'x)$, to prove the generalization of the model over a range of reactions.

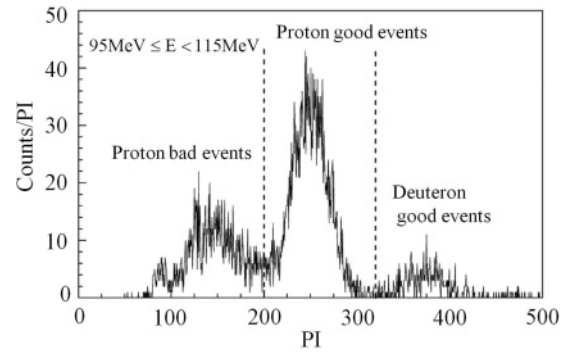

FIG. 3. PI histogram for the $p + {}^{51}$V reactions at 392 MeV in the 95- to 115-MeV energy range.

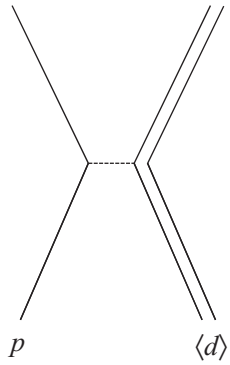

FIG. 4. Scattering $p + d$, where d is treated as an elementary particle.

II. EXPERIMENTS

Experiments were carried out at the Research Center for Nuclear Physics (RCNP), Osaka University. Since the present data were obtained at the same time as $(p, p'x)$ reaction measurements, which were reported in Refs. [17,18], only a brief explanation is given for the experimental procedure here. In the experiments, proton beams of 300 and 392 MeV were provided by the ring cyclotron. Either proton beam was focused on a target in a spot of about 5-mm diameter. The target was set at the center of a vacuum chamber of 1-m diameter. The beam current was collected in a Faraday cup located within a shielding wall about 4 m downstream of the target position. The current was approximately 5 nA on the targets during the data gathering run. A digital current integrator (ORTEC model 439) was used to measure the total charge. The total charge was about 5–10 μC in the forward-angle measurements, and 30–50 μC in the backward-angle measurements. The targets used were ^{12}C, ^{27}Al, ^{51}V, ^{93}Nb, and ^{197}Au, which are all natural metals. Their thicknesses are listed in Table I.

The energy of emitted deuterons was measured with two stacked scintillator spectrometers, which are shown schematically in Fig. 1. Each spectrometer consisted of three thin plastic scintillators and three thick GSO(Ce) scintillators. The first plastic scintillator, having a 15-mm-diameter aperture, served as an active collimator. The second and third plastic

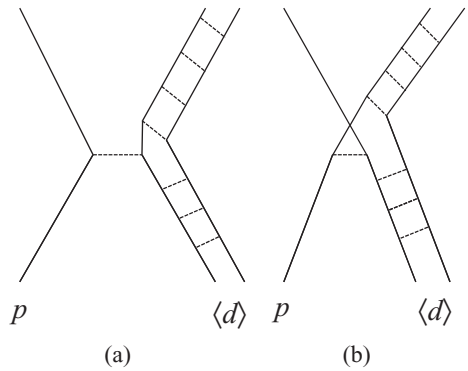

FIG. 5. Scattering $p + d$, where d is treated as a composite particle.

TABLE II. Experimental data used for parameter search.

	Energy (MeV)	Target	Angle
	300	C,Nb,Au	20,30,45,60,75,90,105
(p, d)		Al	25,30,45,60,75,90,105
Present	392	V,Ta,Au	20,30,45,60,75,90,105
result		C	20,30,40,50,75,90,105
		Al	20,35,45,55,75,90,105
		Nb	20,30,45,55,75,90,105
$(p, ^3\mathrm{He})$ [26]	160,200	Co,Au	20,30,40,50,60,80,100,120
(p, α) [27]	160,200	Co,Au	20,30,40,50,60,80,100,120

scintillators were ΔE detectors 1 and 2 mm in thickness, respectively. Two GSO(Ce) crystals were cubic with an edge length of 43 mm, and the final one was a cylinder 60 mm in diameter and 230 mm in length. A total depth of 316 mm was sufficient to stop 400-MeV protons and deuterons. Through experimental studies, deuteron light outputs of GSO(Ce) have been determined [19] as a function of deuteron energy. Energy calibration was performed by referring to proton energy, which was measured by using monoenergetic protons from p-hydrogen elastic scattering off a CH_2 film. Deuteron energy was determined from the light output difference between protons [20] and deuterons. The spectrometers were installed on a goniometer outside the chamber. Deuteron energy spectra were measured at laboratory angles from 20° to 104°.

High-energy deuterons may undergo nuclear reactions before being stopped or may scatter out of the crystal. The ratio between the number of stopped deuterons and the total number of deuterons is referred to as the peak-to-total efficiency of the spectrometer and is necessary to determine absolute cross sections. Thus far, efficiency has been determined as a function of deuteron energy up to 400 MeV [19] in both experiment and simulation calculations.

The DDXs are determined by

$$\frac{d^2\sigma}{d\Omega\, d\varepsilon} = \frac{Y}{P S_t \phi \Delta\Omega \Delta\varepsilon}, \tag{1}$$

where $\Delta\varepsilon$ is the energy bin width required for data reduction, $\Delta\Omega$ is the solid angle of the detector, P is the peak efficiency, S_t is the surface density of the target, and ϕ is the total charge of the incident proton beam. The number of deuterons in $\Delta\epsilon$, which is represented by Y, is obtained by the particle identification (PI) technique. The quantity PI is given by

$$\mathrm{PI} = E_{\mathrm{tot}}^b - (E_{\mathrm{tot}} - \Delta E)^b, \tag{2}$$

where E_{tot} is the total energy deposited in the detector and ΔE is the energy measured in the dE detectors. The parameter b is set at 1.73, which is the optimum value to separate deuterons

TABLE III. Parameters determined for three types of reactions.

	d	t, ^{3}He	α
λ_i (fm)	1.2	1.5	1.7
λ_f (fm MeV/c)	2000	2250	2500

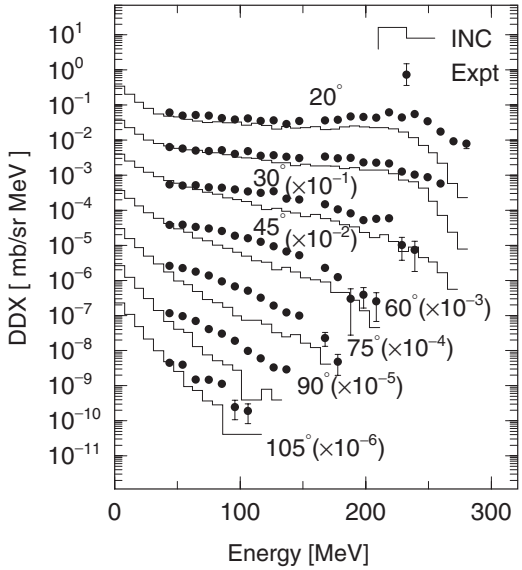

FIG. 6. Energy-angle distributions of the ^{12}C(p, dx) reaction at 300 MeV. Solid lines indicate the present INC calculations. Factors indicated in parentheses are multipliers to avoid data pile up.

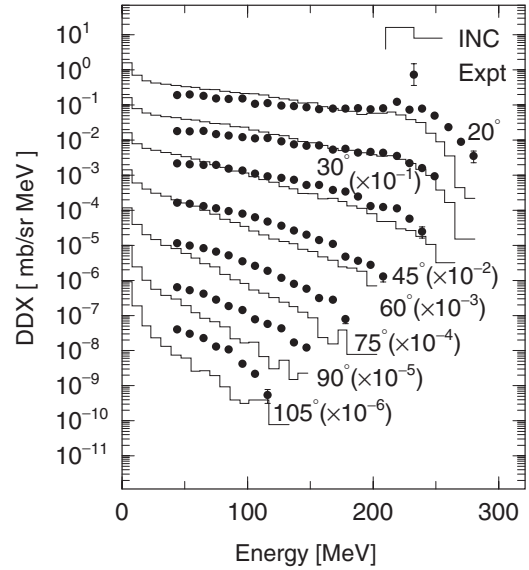

FIG. 8. Same as in Fig. 6 but for the ^{93}Nb(p, dx) reaction.

from protons. A typical example of a two-dimensional PI-$E_{\rm tot}$ plot is shown in Fig. 2 for the case of the p+^{51}V reaction at 392 MeV. Furthermore, Fig. 3 presents an example PI histogram in the 95- to 115-MeV energy range. The number of deuterons is counted by a peak fitting program that can subtract the background noise from the protons.

The systematic error of DDX has been estimated [17,18] to be about 10% in total. The main contributions of this error come from uncertainties in the beam current integration (5%), the target thickness (3–5%), and the proton-deuteron separation in PI analyses (7% or less). Statistical errors were less than 1%.

III. THEORETICAL MODEL

A. INC

The INC model used presently was detailed in Ref. [18]. Thus, only a brief description is given here. The ground state of the target nucleus has a Woods-Saxon shape density distribution and a square-well potential V_0 of 45 MeV in depth. Fermi momentum is calculated by considering nuclear binding energy. The nuclear radius R_0 and the diffuseness a_0 are calculated by using Negele's parameters [21],

$$R_0 = (0.978 + 0.0206A^{1/3})^{1/3}A^{1/3} \quad \text{fm}, \tag{3}$$

$$a_0 = 0.54 \quad \text{fm}. \tag{4}$$

The cutoff of the nuclear radius $R_{\rm max}$ has been chosen as $R_{\rm max}$= $R_0 + 8a_0$. Nucleon-nucleon cross sections and angular

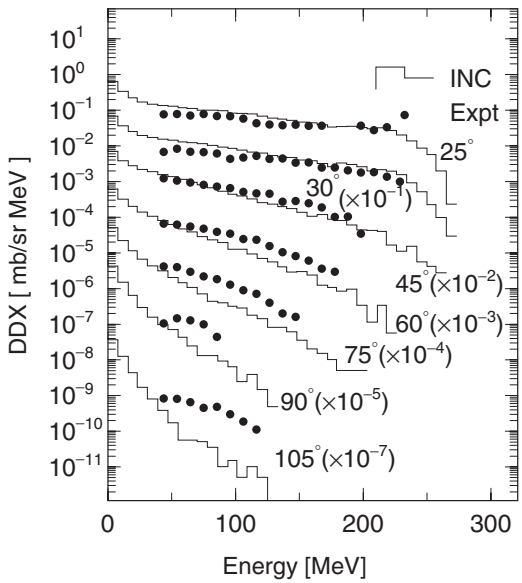

FIG. 7. Same as in Fig. 6, but for the ^{27}Al(p, dx) reaction.

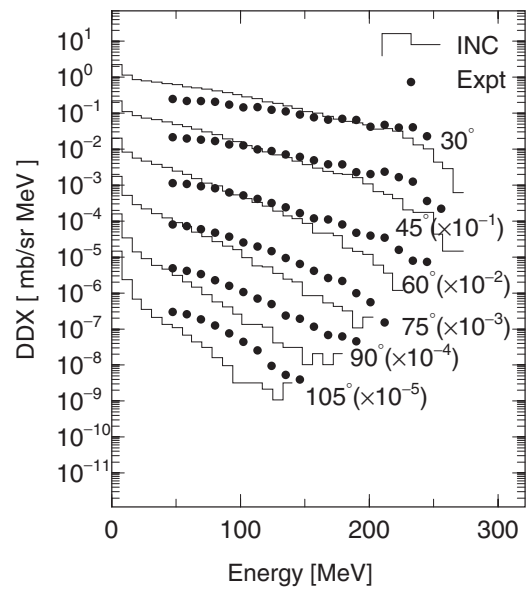

FIG. 9. Same as in Fig. 6 but for the ^{197}Au(p, dx) reaction.

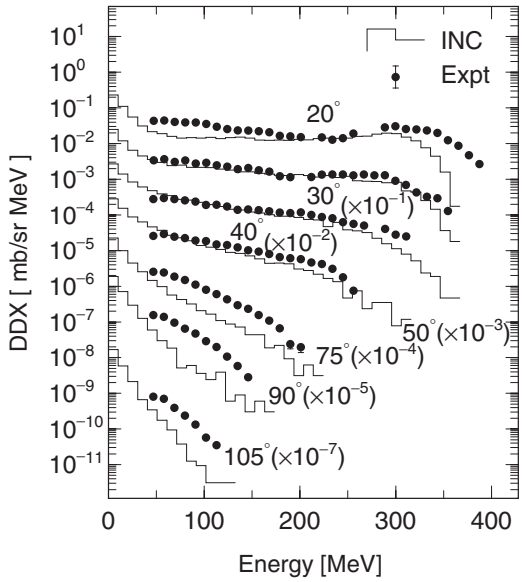

FIG. 10. Same as in Fig. 6 but for the ^{12}C(p, dx) reaction at 392 MeV.

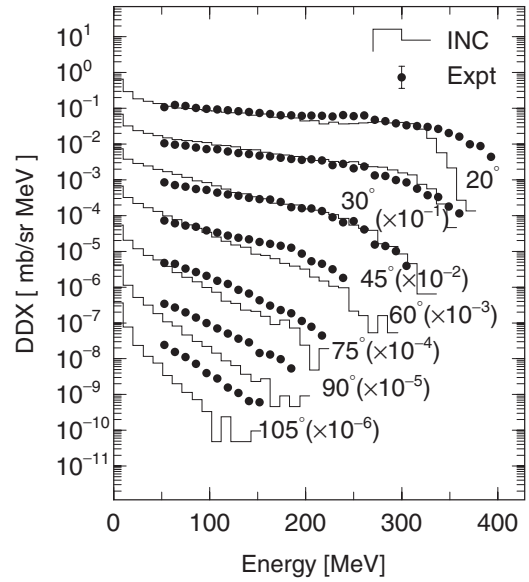

FIG. 12. Same as in Fig. 6 but for the ^{51}V(p, dx) reaction at 392 MeV.

distributions are given by Cugnon *et al.*'s parameters [22]. The occurrence of collisions is judged from Pauli blocking, which forbids collisions leading to nucleons having momenta smaller than the Fermi momentum. Nucleons under the Fermi sea are treated as spectators and are not traced in terms of their positions. A nucleon reaching the nuclear surface is assumed to be emitted when its energy is higher than the threshold. Reflection or refraction by the changing nuclear potential is not included. The model assumes the nucleus to be at equilibrium when all of the cascade particles that are not emitted fall below the threshold energies. At the end of the cascade phase, the residual nucleus deexcites through evaporation, and a statistical technique was used to compute the evaporation of nucleons and clusters, such as deuterons and α particles. The subsequent evaporation calculations were performed with the computer code GEM [23]. The present INC model computes the reaction cross section by multiplying the geometric cross section by the ratio between the number of incident protons that interact in the target nucleus and the total number of trials.

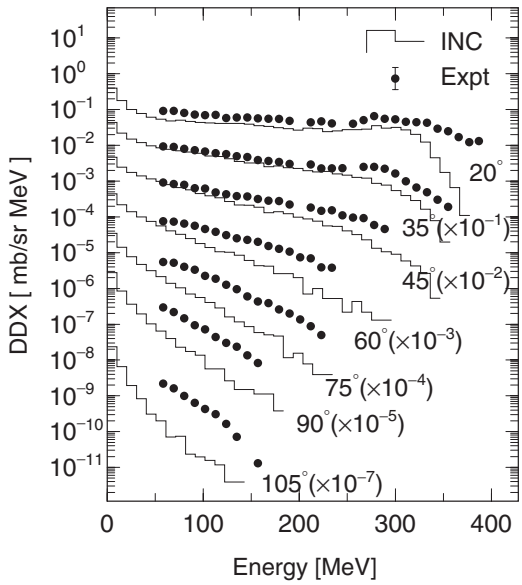

FIG. 11. Same as in Fig. 6 but for the ^{27}Al(p, dx) reaction at 392 MeV.

B. Extension of INC model to include nucleon correlations

There are several processes responsible for deuteron formation in the (p, dx) reaction. In this work, we consider only indirect pickup and knockout processes. To incorporate these processes, the standard INC model is extended to include nucleon correlation in both the initial and final states of the reaction. We ignore the direct pickup process, which excites a shell-model-like state of the residual nucleus, since that process is impossible to handle within the INC framework. We also ignore the direct deuteron formation process via

$$p + \langle N \rangle \rightarrow d + \pi \quad \text{or} \quad \gamma. \tag{5}$$

In the higher-energy domain, the direct deuteron formation process [15] will become significant, which is accompanied by the pion production $p + \langle d \rangle \rightarrow d + \pi$; however, this is negligible in the present energy range. The process accompanying γ emission also has negligible intensity. The contribution of the evaporation process is excluded.

The initial-state correlation appears in the ground state of the target nucleus and is responsible for the knockout process; $p + \langle d \rangle \rightarrow p + d$. In addition to the single-particle state, the nuclear ground state includes a cluster state, such as a deuteron and an α particle, as a higher-order component of the wave function. The ground-state wave function $|\mathrm{Gr}\rangle$ for the A-nucleon system is expressed by the superposition of various

cluster states as

$$|\mathrm{Gr}\rangle = c_1|(\mathrm{s.p.})_A\rangle + c_2|(\mathrm{s.p.})_{A-2}(d)_2\rangle + c_3|(\mathrm{s.p.})_{A-4}(\alpha)_4\rangle + \cdots. \quad (6)$$

Many repetitions of the INC calculation will simulate this superposition of the wave function. Note that only the single-particle state $|(\mathrm{s.p.})_A\rangle$ has been assumed in not only the ordinal INC model but also QMD and other nuclear reaction theories that describe spallation reactions.

The underlying physics is based on the existence of a preformed cluster inside a target nucleus. In a previous study, a preformed deuteron was assumed to be a single elementary particle. In such a case, the diagram of the $p + \langle d \rangle$ scattering process can be depicted as Fig. 4 and accounting for the experimentally observed forward-peaked angular distribution is difficult in (p, dx) reactions. Note that the actual process is more complex than the present model; for instance, in reality an integration process [24] is included that stimulates excitation of spin-forbidden states.

In this study, the preformed cluster is considered to be a composite of nucleons but not an elementary particle. A schematic of the deuteron knockout process is shown in Fig. 5, where (a) corresponds to a direct term and (b) to the exchange term. Note that the exchange process is essential for explaining the forward peak in the angular distribution. Since a high-energy cluster is produced via interference, this cannot be interpreted from a classical viewpoint. The artificial criterion at the initial state of reaction is defined through a parameter λ_i as

$$r_{\mathrm{nm}} \leqslant \lambda_i, \quad (7)$$

where r_{nm} is the distance between two nucleons. If two nucleons are found near the nth nucleon, that is,

$$r_{\mathrm{nm}} \leqslant \lambda_i \quad \text{and} \quad r_{\mathrm{nl}} \leqslant \lambda_i, \quad (8)$$

a cluster having a mass of 3 is assumed to be produced. Similarly, we treat a cluster up to an α particle. In this process,

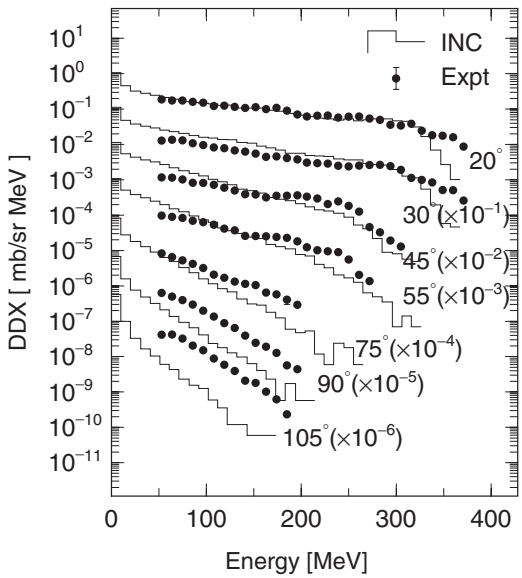

FIG. 13. Same as in Fig. 6 but for the ^{93}Nb(p, dx) reaction at 392 MeV.

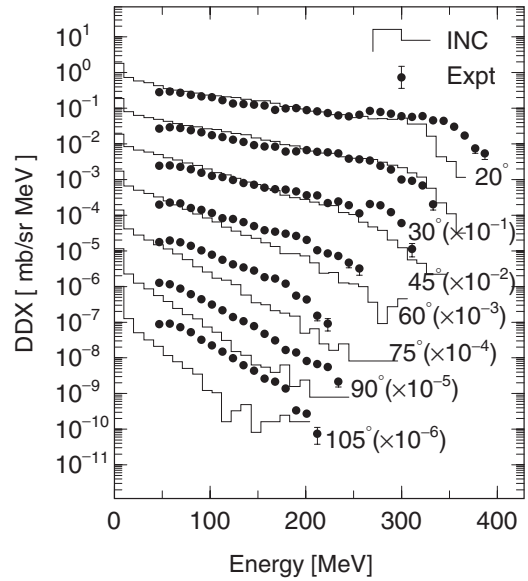

FIG. 14. Same as in Fig. 6 but for the ^{197}Au(p, dx) reaction at 392 MeV.

energy conservation is assumed to be fulfilled. The emission direction is determined by the sum of the momentum vectors of all nucleons.

The final-state correlation is responsible for the indirect pickup or coalescence process. The coalescence process is deuteron formation by a proton and a neutron emerging from the nuclear surface. Indirect pickup is that process when a cascade proton picks up a bound neutron. Such pickup is a well-known direct process induced by an incident fast nucleon. Here, we ignore these differences and call all such processes pickup.

The pickup process is dominant in the low-energy part of the spectrum above the evaporation regime. We assumed that,

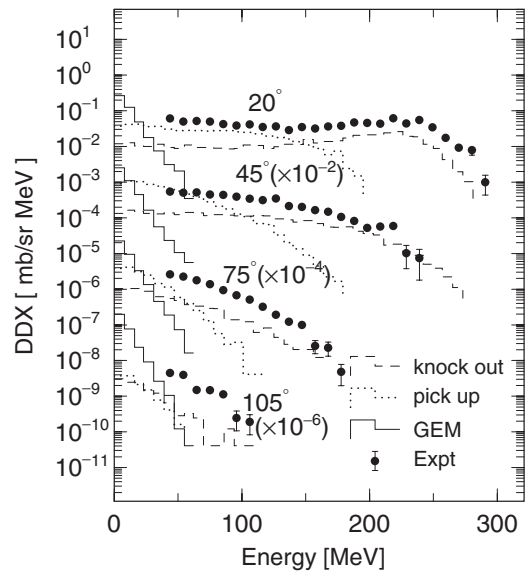

FIG. 15. Contributions of knockout (broken lines), pickup (dotted lines), and evaporation (solid lines) to the ^{12}C(p, dx) reaction at 300 MeV.

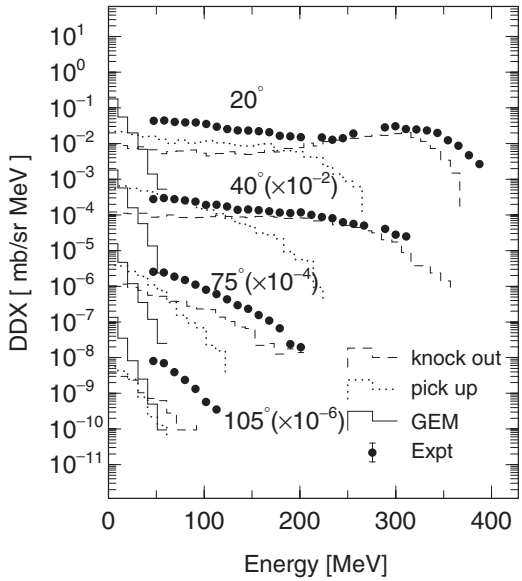

FIG. 16. Same as in Fig. 15 but for the ^{12}C(p, dx) reaction at 392 MeV.

through this process, a cluster is produced when two or more nucleons are found within a limited phase space in the final state. Nonexcited nucleons below the Fermi level, in addition to excited nucleons, can be picked up by a leading particle at the nuclear surface of $R_{\max}$. This assumption is similar to that in the Iwamoto-Harada model [25] but differing from that in coalescence models, which assume that an outgoing cluster is formed by nucleons excited above the Fermi level. The clustering criterion can be written through a parameter λ_f in the form

$$r_{\rm nm}\ p_{\rm nm} \leqslant \lambda_f, \tag{9}$$

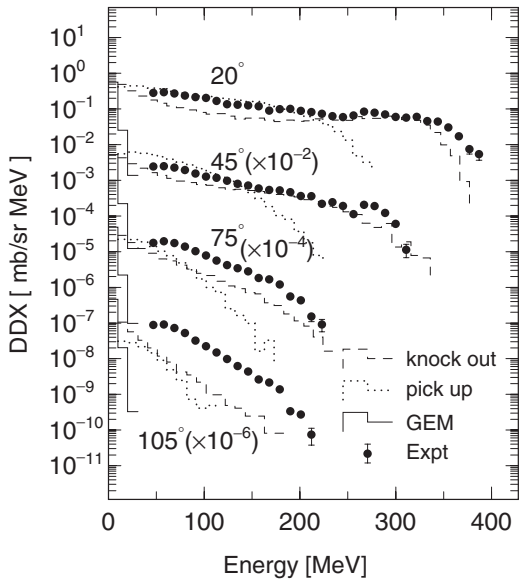

FIG. 17. Same as in Fig. 15 but for the ^{197}Au(p, dx) reaction at 392 MeV.

where $r_{\rm nm}$ and $p_{\rm nm}$ represent the distances between nucleons in phase space. Since the opportunity exist to find more nucleons in the neighborhood of the emitting one, heavier clusters up to an α particle are considered as in the case of the initial state. In this process, momentum conservation is assumed to hold.

The parameters λ_i and λ_f are chosen in order to reproduce spectral DDXs observed experimentally. Calculated (p, dx) spectra are affected by the inclusion of reactions emitting tritons and helium ions. Although beam energies are low, experimental data on $(p, ^3\mathrm{He}x)$ [26] and $(p, \alpha x)$ [27] reactions are available at 160 and 200 MeV. We, therefore, include these data for searching critical parameters dependent on the mass of the emitting ions from the deuteron to the α particle. Three parameter sets are thus determined in order to obtain the best fit to the data. These sets are summarized in Table II. In the calculation, cluster formation candidates are searched for with the first priority given to α, the second priority to ^{3}He and tritons, and the last priority to deuterons. If the total energy is positive and can tunnel through the Coulomb barrier, the candidate cluster is emitted. If this candidate fails, the next one is tested. In Table III critical parameters determined in this study are listed. Results of comparisons between the calculated and observed data are discussed in the next section.

C. QMD

QMD calculation was performed with the PHITS code. In QMD, nuclear reactions are calculated as the time development of a $p + \mathrm{A}$ system. The motion of the nth nucleon having position R_n and momentum P_n is assumed to be given by the Newtonian equations

$$\dot{R}_n = \frac{\partial H}{\partial P_n}, \quad \dot{P}_n = -\frac{\partial H}{\partial R_n}, \tag{10}$$

where H is the Hamiltonian consisting of the relativistic kinetic+mass energy and Skyrme-type effective N-N interaction, the Coulomb and symmetry energy terms of the total system including the projectile and the target. In addition to this, nucleon-nucleon scattering is calculated for the time development. All parameters values used were default values of the PHITS QMD code and were the bulk properties of the nucleus determined over a wide mass range. The in-medium nucleon-nucleon scattering was calculated in the same manner as that used in the present INC computation. Pauli blocking was checked after each scattering with a blocking probability calculation of the phase-space occupancy [28].

Once the equilibrium was attained, evaporation calculations were performed for nucleons and clusters with the GEM [23] computer code, as in the case of INC.

IV. RESULTS AND DISCUSSION

A. Deuteron spectral DDX and improved INC

All the data are shown in Figs. 6–14.

Circles in the figures depict experimental results of deuteron spectral DDXs from (p, dx) reactions. Statistical errors are indicated by vertical lines on the data. The spectra are

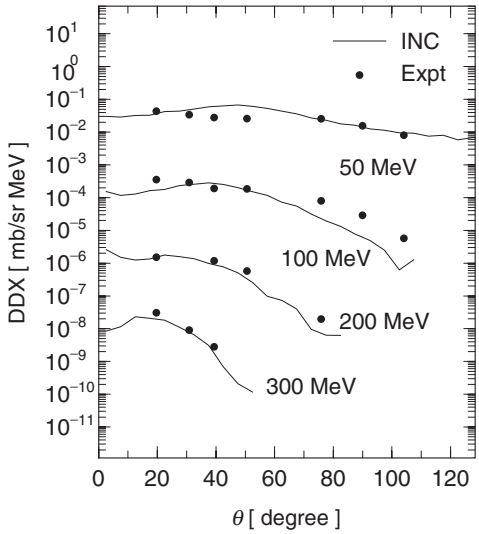

FIG. 18. Angular distributions for the ^{12}C(p, dx) reaction at 392 MeV.

multiplied by the indicated factors for display purposes. Overall, spectra are characterized by a high-energy portion whose intensity decreases sharply with increasing angle. In the case of a light target, ^{12}C, broad peaks having a width of about 100 MeV are present in the highest-energy part at 20°, where the deuteron energies are very close to the proton beam energy. These peaks could be indicative of the quasifree proton-deuteron scattering (QFS) discussed in previous work [13–16]. In contrast, no prominent bumps are seen for medium and heavy targets. These features are very similar to those of $(p, p'x)$ reactions [17,18], but the magnitudes are roughly 1/10 of those for $(p, p'x)$ reactions.

The solid lines in the figures show the present INC results. Overall, they are in good agreement with the experimental data. However, the highest ends of the spectra at 20° are underestimated. These high-energy spectra are governed by

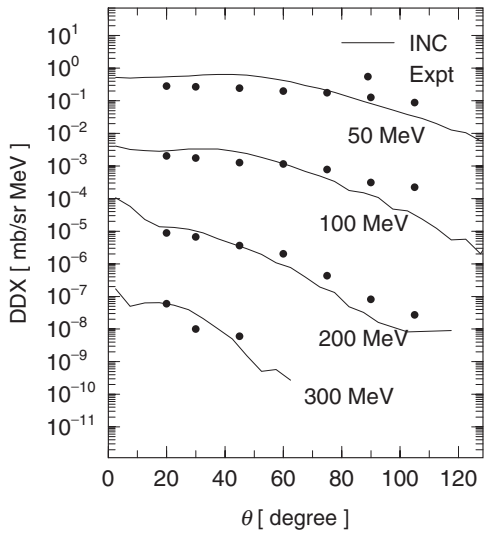

FIG. 19. Angular distributions for the ^{197}Au(p, dx) reaction at 392 MeV.

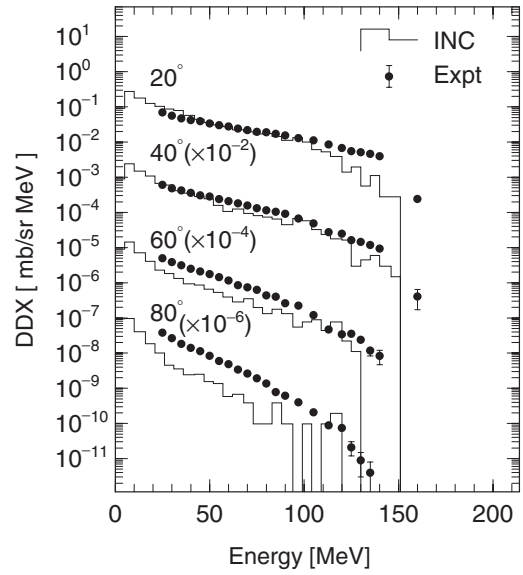

FIG. 20. Same as in Fig. 6 but for the ^{59}Co$(p, x^3$He) reaction at 200 MeV. Experimental data are taken from Ref. [26].

the direct pickup process, which is not presently considered in the model. The underprediction tends to increase at larger angles and for heavier targets. However, this trend should be considered as a general aspect of INC calculation [18], due to the assumption of a straight trajectory of nucleons.

The contribution from each of the knockout, indirect pickup, and evaporation processes is indicated in Figs. 15 and 16 for the ^{12}C$(p, p'x)$ reactions at 300 and 392 MeV, respectively. Deuterons from the knockout process appear for wide energy and angle ranges. In particular, the contribution from the knockout process is dominant in the higher-energy domain at forward angles, the region in which the QFS peak has been suggested to exist. The single-step knockout process, that is, $p + \langle d \rangle \rightarrow p + d$, is consistent with the QFS. The

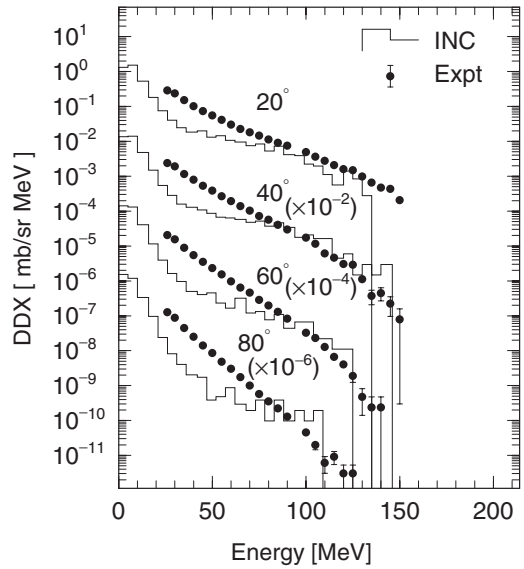

FIG. 21. Same as in Fig. 6 but for the ^{59}Co$(p, x\alpha)$ reaction at 200 MeV. Experimental data are taken from Ref. [27].

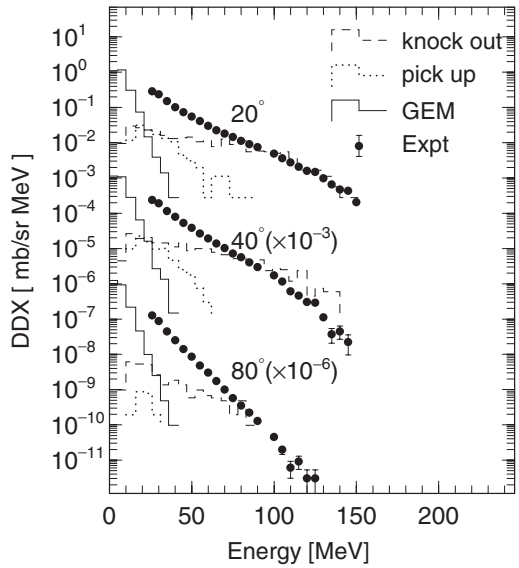

FIG. 22. Same as in Fig. 6 but for the ^{59}Co$(p, x\alpha)$ reaction at 200 MeV. Experimental data are taken from Ref. [27].

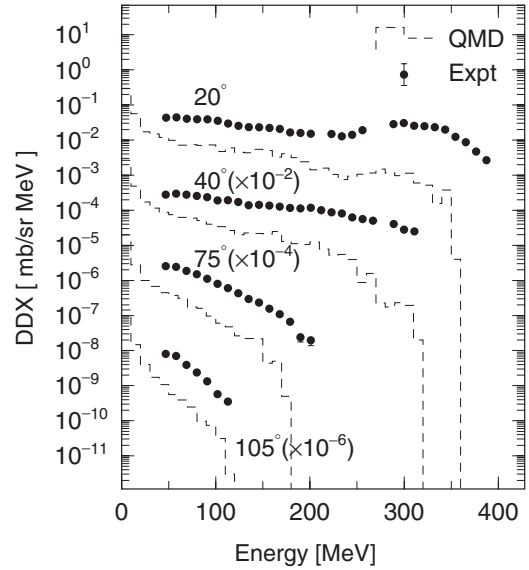

FIG. 24. Results of QMD (dashed lines) and observation for the ^{12}C(p, xd) reaction at 392 MeV.

indirect pickup process contributes largely in the middle to lower portions of the energy spectra. At 105°, both processes appear very similar to each other. The evaporated deuterons are observed in the lowest-energy range and are dominant below 20 MeV. The same graphs are shown in Fig. 17 for the ^{197}Au$(p, p'x)$ reaction at 392 MeV. In the case of a heavy target, the overall trends are almost same as those in the case of a light target.

Typical angular distributions of emitted deuterons are shown in Figs. 18 and 19 for the ^{12}C(p, dx) and ^{197}Au(p, dx) reactions at 392 MeV. At high emission energies, the observed distributions are forward peaked, and the distributions become more isotropic with decreasing energy. The present INC gives overall accounts of the measured angular distributions. In particular, that the forward-peaked distributions are reproduced well is worth emphasizing.

B. Test of improved INC with other reactions

As described in Sec. II, the parameter search was completed by including $(p,^3\text{He})$ and (p, α) reactions. In this section, we discuss these results. Moreover, further tests of the present INC was performed with the $(d, d'x)$ reactions. The results for these reactions are also discussed here.

In Figs. 20 and 21, the solid lines are the current calculated results, and the dots are experimental DDX data for the $(p,^3\text{He}x)$ [26] and $(p, \alpha x)$ [27] reactions on ^{59}Co at 200 MeV. On the whole, these figures give a better account of the observed trends with changing angles and energies

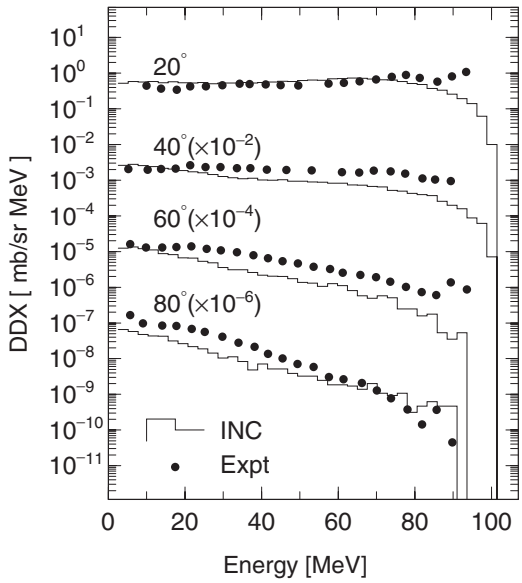

FIG. 23. Same as in Fig. 6 but for the ^{27}Al(d, xd') reaction at 100 MeV. Experimental data are taken from Ref. [29].

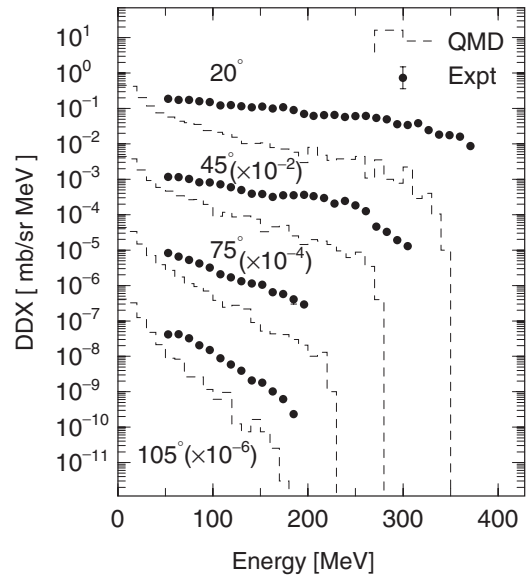

FIG. 25. Same as in Fig. 24 but for the ^{93}Nb(p, xd) reaction at 392 MeV.

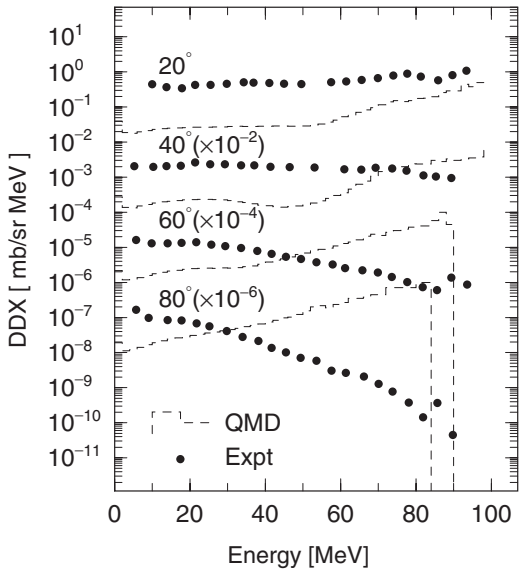

FIG. 26. Same as in Fig. 6 but for the ^{27}Al(d, xd') reaction at 100 MeV. Experimental data are taken from Ref. [30].

for both reactions. Each of the knockout, indirect pickup, and evaporation processes are indicated in Fig. 22 for the ^{59}Co$(p, \alpha x)$ reaction. The figure implies that α emission is governed by the knockout process and that the pickup process is minor. This result is consistent with the conclusion in a previous experimental study [29] of $(p, \alpha x)$ reactions. Figure 23 shows that the current model can describe the deuteron inelastic scattering, specifically, the ^{27}Al$(d, d'x)$ reactions at 100 MeV [30].

The values of λ_i and λ_f listed in Table III are dependent on the (p, dx), $(p, ^3\mathrm{He}x)$, and $(p, \alpha x)$ reactions at 160–200 MeV, but independent of the incident and emission energies, and the mass of the target nucleus. The larger values for α particles than for other clusters might be attributable to the fact that α particles are more rigid than other light clusters. Although the strength of the final-state interaction is sensitive to the target, the sharp dependence might disappear at very high excitation energies.

C. QMD GEM calculation of (p, dx) and $(d, d'x)$ reactions

Figures 24 and 25 show two representative selections for comparison between the QMD GEM results, indicated by long-dashed lines, and observations for the ^{12}C(p, dx) and ^{91}Nb(p, dx) reactions at 392 MeV. Overall, the calculated results are of smaller magnitude than those from observations. The QMD calculations appear to decrease faster than the observations for the high-energy portions of the forward-angle spectra. In the highest-energy domain, QMD tends to underpredict observations by two to three orders of magnitude. With decreasing deuteron energy, the discrepancy becomes smaller. However, QMD still underestimates the experimental results at approximately 50 MeV, the lowest observation energy. The contribution of evaporation seems to be prominent in the energy range lower than about 30 MeV. QMD calculations were also performed for the ^{27}Al$(d, d'x)$ reaction at 100 MeV (Fig. 26). However, the results imply that the QMD treatment of deuterons is unsuitable, although QMD succeeded in describing heavy-ion reactions.

The deuteron formation in QMD may be understood to be coalescence-like in the final state. Clustering occurs via only the Skyrme-type two-body potential, which is introduced to produce a nuclear mean field. The potential does not induce any strong correlations that usher in cluster formation. Note that the interference plays an essential role in clustering, since the system is in an unbound energy state initially. For instance, the capture goes through an unbound state of a pn pair and then falls down to the bound state: $p + n \rightarrow pn \rightarrow d + \gamma$. Although nucleons are referred to as wave packets in QMD, their wave properties are not considered, and the characteristics of a wave function cannot be described, such as diffraction and interference. As the result, QMD shows remarkable underpredictions for high-energy deuterons but reasonable accounts at lower energies.

V. CONCLUSION

Deuteron production from intermediate-energy proton-nucleus interactions was investigated. Double-differential cross sections were measured for (p, dx) reactions at 300 and 392 MeV on five target nuclei. To explain our observations, we proposed a model including nucleon correlations at the initial- and final-state interactions for knockout and pickup processes, respectively, on the basis of the intranuclear cascade model. The model can give a reasonable account of the trends in the observed distributions with changes in both target mass and incident proton energy. The model can also reproduce distributions of other cluster productions and deuteron inelastic spectra satisfactorily.

ACKNOWLEDGMENTS

We thank the staff of the RCNP cyclotron facility for technical support in the experiments.

[1] H. Iwase, K. Niita, and T. Nakamura, J. Nucl. Sci. Technol. **39**, 1142 (2002).
[2] J. Allison *et al.*, IEEE Trans. Nucl. Sci. **53**, 270 (2006), and references therein.
[3] P. E. Hodgson and E. Běták, Phys. Rep. **374**, 1 (2003).
[4] A. Ono, H. Horiuchi, T. Maruyama, and A. Ohnishi, Phys. Rev. C **47**, 2652 (1993).
[5] S. F. Butler and C. A. Person, Phys. Rev. **129**, 836 (1963).
[6] A. Schwarzschild and Č. Zupančič, Phys. Rev. **129**, 856 (1963).
[7] H. H. Gutbrod, A. Sandoval, P. J. Johansen, J. Gosset, W. G. Meyer, G. D. Westfall, and R. Stock, Phys. Rev. Lett. **37**, 667 (1976).
[8] J. Cugnon and C. Volant, Zeitschrift für Phys. A **334**, 435 (1989).

[9] A. Letourneua *et al.*, Nucl. Phys. A **712**, 133 (2002).
[10] A. Boudard, J. Cugnon, and C. Volant, Nucl. Phys. A **740**, 195 (2004).
[11] A. Budzanowski *et al.*, Phys. Rev. C **78**, 024603 (2008).
[12] A. Budzanowski *et al.*, Phys. Rev. C **80**, 054604 (2009).
[13] W. N. Hess and B. J. Moyer, Phys. Rev. **101**, 337 (1956).
[14] R. J. Sutter *et al.*, Phys. Rev. Lett. **19**, 1189 (1967).
[15] L. S. Azhgirei *et al.*, Nucl. Phys. A **195**, 581 (1972).
[16] P. J. Riley *et al.*, Phys. Rev. C **17**, 1881 (1978).
[17] T. Kin *et al.*, Phys. Rev. C **72**, 014606 (2005).
[18] H. Iwamoto *et al.*, Phys. Rev. C **82**, 034604 (2010).
[19] F. Saiho, T. Kin, S. Hohara, G. Wakabayashi, N. Ikeda, Y. Uozumi, M. Imamura, Y. Yamashita, M. Matoba, and N. Koori, Nucl. Instrum. Methods A **537**, 594 (2005).
[20] K. Anami *et al.*, Nucl. Instrum. Methods A **404**, 327 (1998).
[21] J. W. Negele, Phys. Rev. C **1**, 1260 (1970).
[22] J. Cugnon, D. D'Hote, and J. Vandermeulen, Nucl. Instrum. Methods B **111**, 215 (1996).
[23] S. Furihata, Nucl. Instrum. Methods B **171**, 251 (2000).
[24] R. Ent *et al.*, Phys. Rev. Lett. **62**, 24 (1989).
[25] A. Iwamoto and K. Harada, Phys. Rev. C **26**, 1821 (1982); Nucl. Phys. **419**, 472 (1984).
[26] A. A. Cowley, G. J. Arendse, G. F. Steyn, J. A. Stander, W. A. Richter, S. S. Dimitrova, P. Demetriou, and P. E. Hodgson, Phys. Rev. C **55**, 1843 (1997).
[27] A. A. Cowley, G. J. Arendse, J. W. Koen, W. A. Richter, J. A. Stander, G. F. Steyn, P. Demetriou, P. E. Hodgson, and Y. Watanabe, Phys. Rev. C **54**, 778 (1996).
[28] G. F. Bertch and S. Das Gupta, Phys. Rep. **160**, 189 (1988).
[29] J. Mabiala, A. A. Cowley, S. V. Förtsch, E. Z. Buthelezi, R. Neveling, F. D. Smit, G. F. Steyn, and J. J. Van Zyl, Phys. Rev. C **79**, 054612 (2009).
[30] S. V. Förtsch *et al.*, J. Nucl. Sci. Technol. Suppl. **2**, 792 (2002).